Lipoprotein-Based Nanoparticles Rescue the Memory Loss of Mice with Alzheimer's Disease by Accelerating the Clearance of Amyloid-Beta

Qingxiang Song,[†] Meng Huang,[†] Lei Yao,[†] Xiaolin Wang,[†] Xiao Gu,[†] Juan Chen,[‡] Jun Chen,[§] Jialin Huang,[†] Quanyin Hu,[§] Ting Kang,[§] Zhengxing Rong,[†] Hong Qi,[†] Gang Zheng,[‡,*] Hongzhuan Chen,[†,*] and Xiaoling Gao[†,*]

[†]Department of Pharmacology, Institute of Medical Sciences, Shanghai Jiao Tong University School of Medicine, 280 South Chongqing Road, Shanghai 200025, PR China, [‡]Department of Medical Biophysics and Ontario Cancer Institute, University of Toronto, Toronto, Ontario M5G 1L7, Canada, and [§]Department of Pharmaceutics, Key Laboratory of Smart Drug Delivery, Ministry of Education & PLA, School of Pharmacy, Fudan University, 826 Zhangheng Road, Shanghai 201203, PR China

ABSTRACT Amyloid-beta (Aβ) accumulation in the brain is believed to play a central role in Alzheimer's disease (AD) pathogenesis, and the common late-onset form of AD is characterized by an overall impairment in Aβ clearance. Therefore, development of nanomedicine that can facilitate Aβ clearance represents a promising strategy for AD intervention. However, previous work of this kind was concentrated at the molecular level, and the disease-modifying effectiveness of such nanomedicine has not been investigated in clinically relevant biological systems. Here, we hypothesized that a biologically inspired nanostructure, apolipoprotein E3—reconstituted high density lipoprotein (ApoE3—rHDL), which presents high binding affinity to Aβ, might serve as a novel nanomedicine for disease modification in AD by accelerating Aβ clearance. Surface plasmon resonance, transmission electron microscopy, and co-immunoprecipitation analysis showed that ApoE3—rHDL demonstrated high binding affinity to both Aβ monomer and oligomer. It also accelerated the microglial, astroglial, and liver cell degradation of Aβ by facilitating the lysosomal transport. One hour after intravenous administration, about 0.4% ID/g of ApoE3—rHDL gained access to the brain. Four-week daily treatment with ApoE3—rHDL decreased Aβ deposition, attenuated microgliosis, ameliorated neurologic changes, and rescued memory deficits in an AD animal model. The findings here provided the direct evidence of a biomimetic nanostructure crossing the blood—brain barrier, capturing Aβ and facilitating its degradation by glial cells, indicating that ApoE3—rHDL might serve as a novel nanomedicine for disease modification in AD by accelerating Aβ clearance, which also justified the concept that nanostructures with Aβ-binding affinity might provide a novel nanoplatform for AD therapy.

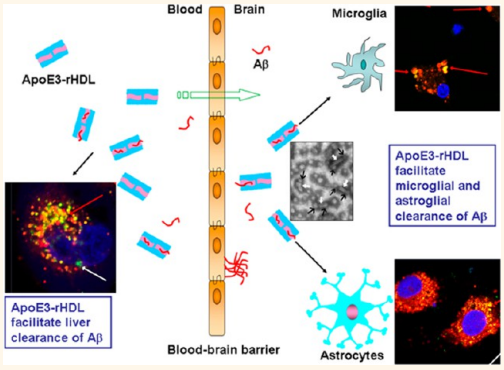

KEYWORDS: reconstituted high density lipoprotein · nanomedicine · amyloid beta · apoliporpotein E · clearance · Alzheimer's disease

Alzheimer's disease (AD), the most common form of dementia, is now representing one of the largest unmet medical needs. According to the World Alzheimer Report 2009, more than 36 million people worldwide are living with dementia, with numbers doubling every 20 years to 66 million by 2030, and 115 million by 2050. The worldwide costs of dementia (US$604 billion in 2010) amount to more than 1% of global GDP, and will continue to grow during the global aging process. If nothing is done, the personal, economic, and societal toll of the ongoing and growing AD epidemic will be immense. But until now, there is no effective treatment that delays the onset or slows the progression of AD. Therefore, development of strategies for AD therapy are among the most challenging and timely areas in modern medicine.

The pathological hallmarks in AD brain are the senile plaques formed by amyloid-beta (Aβ) aggregation and the neurofibrillary tangles formed by hyperphosphorylated tau.[1]

* Address correspondence to gzheng@uhnresearch.ca, hongzhuan_chen@hotmail.com, shellygao1@sjtu.edu.cn.

Received for review November 10, 2013 and accepted February 17, 2014.

Published online February 17, 2014
10.1021/nn4058215

Genetic, pathological and biochemical clues suggested that Aβ accumulation in the brain induced by an imbalance between its production and clearance plays a central role in AD pathogenesis. Aβ peptides are generated by the sequential proteolytic processing of amyloid β precursor protein (APP) by the β- and γ-secretase, forming Aβ fragments with varying number of amino acids ranging from 36 to 42.[2] It is widely acknowledged that the accumulation of soluble Aβ into toxic oligomers and amyloid plaques initiates the pathogenic cascade leading to tau protein hyperphosphorylation, intracellular neurofibrillary tangles, synaptic dysfunction, neuronal death, and, ultimately, loss of cognitive function.[3] Development of nanostructures that can interfere with the polymerization of Aβ has been of particular interest.[4−7] However, recent work demonstrated that the common late-onset form of AD is characterized by an overall impairment in Aβ clearance but not in Aβ production.[8,9] Therefore, Aβ clearance are being actively pursued as disease modifying therapies in AD.[10−12]

Clearance of brain Aβ with Aβ-specific antibodies is one of the most efficient ways, but is still associated with autoimmunity-related adverse effects.[13] Development of nanostructures that can facilitate Aβ clearance might represent a novel strategy for AD therapy. Previous work suggested that nanostructures with Aβ-binding affinity holds great potential in facilitating Aβ clearance by capturing circulating Aβ from blood and redirecting the peptide to hepatic macrophages for destruction.[4] Theoretically, nanostructures with both Aβ-binding affinity and blood−brain barrier (BBB) permeability might also capture Aβ in the brain interstitial fluid and facilitate its degradation in the central nervous system (CNS) by glial cells. However, previous work of this kind mainly remained at the molecular level, and the disease-modifying effectiveness of such nanomedicines has not been investigated in clinically relevant biological systems.[7]

Lipoproteins, natural nanoparticles, play a well-recognized biological role and are highly suitable as a nanoplatform for medical diagnostics and therapeutics. High-density lipoprotein (HDL), the smallest lipoprotein, is of particular interest, because of their ultrasmall size and favorable surface properties. Specifically, HDL subtype with apolipoprotein E (ApoE) as the apolipoprotein component, exhibits high binding affinity to Aβ and has been claimed to facilitate the degradation of Aβ in an ApoE isoforms (E2 > E3 > E4)-dependent manner.[9,14] Interestingly, APOE ε4 allele is by now the strongest genetic risk factor for late-onset, sporadic AD,[9] and individuals carrying the ε4 allele are at higher risk of AD compared with those carrying the more common ε3 allele. AD patients appeared to have impairment in the ApoE−lipoprotein-mediated Aβ binding and antiamyloidogenesis.[15,16] In contrast, induction of ApoE production and lipidation by retinoid X receptors agonist, bexarotene, seemed to facilitate Aβ clearance and reverse deficits in AD mouse models.[12] Such evidence strongly suggested that ApoE−HDL might serve as a natural nanostructure that plays a key role in Aβ degradation. Therefore, we hypothesized that the biologically inspired nanostructure, ApoE-reconstituted HDL (ApoE−rHDL), especially those with higher Aβ-binding affinity such as ApoE3−rHDL, might serve as a novel nanomedicine for disease modification in AD by accelerating Aβ clearance.

To justify this hypothesis, in this work, ApoE3, the most predominant ApoE isoform found in healthy population, was utilized as the apolipoprotein component for the construction of ApoE−rHDL. Previous work has witnessed ApoE-mediated brain delivery of both polysorbate 80-coated poly(*n*-butyl cyanoacrylate) (PBCA) nanoparticles and ApoE-conjugated albumin nanoparticles.[17,18] Therefore, in addition to its Aβ-binding affinity, ApoE3−rHDL might also possess the ability to cross the BBB. It was expected to exert disease-modifying effects *via* partially penetrate through the BBB and facilitate intracerebral Aβ clearance by glia-mediated degradation. Those that did not cross the BBB might also bind to Aβ in the circulation and redirect the peptide to the liver for degradation. Here we performed both *in vitro* and *in vivo* experiments to study this possibility and reported the remarkable disease-modifying effects of this biomimetic nanomedicine. Our work also tried to justify the concept that nanostructures with Aβ-binding affinity might serve as a novel nanoplatform for the treatment of AD.

RESULTS AND DISCUSSION

Formation of ApoE3−rHDL. ApoE3−rHDL was prepared by self-assembly from lipid free ApoE3 and phospholipid vesicles *via* a three-step process:[19] (1) preparation of a lipid film by drying a chloroform solution of 1,2-dimyristoyl-*sn*-glycero-3-phosphocholine (DMPC) in a glass round-bottom flask under vacuum desiccation; (2) formation of DMPC liposome by hydrating the lipid film with phosphate buffered saline (PBS) followed by a probe ultrasound treatment; (3) formation of ApoE3−rHDL by incubating lipid-free ApoE3 with the liposome solution. Compared with native low-density lipoprotein and HDL that obtained from pooled fresh human plasma,[20] ApoE3−rHDL here prepared from commercially available synthetic lipids and recombinant apolipoprotein can avoid the danger of transmitting infectious/pathogenic agents from the original human material and is also much easier for scaling-up and reproducibility. Three main isoforms have been described for human ApoE (ApoE2, ApoE3 and ApoE4), among which ApoE3 was chosen for rHDL preparation because ApoE3 is considered as the "wild-type" isoform in human due to its high allelic frequency and lack of strong association with a human disease phenotype. In contrast, ApoE2 is defective for receptor

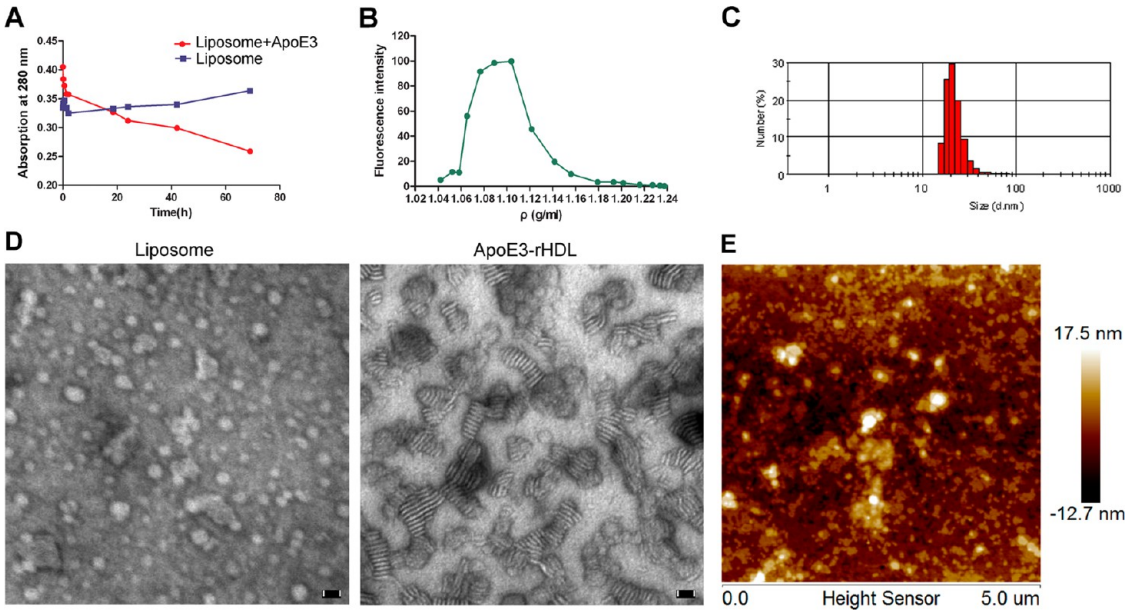

Figure 1. Preparation and characterization of apolipoprotein E3-reconstituted high density lipoprotein (ApoE3−rHDL): (A) Change of 280 nm absorption of DMPC liposome in the presence or absence of ApoE3; (B) distribution of 1,1′-dioctadecyl-3,3,3′,3′-tetramethylindocarbocyanine perchlorate-labeled ApoE3−rHDL at different density fractions; (C) particle size distribution of ApoE3−rHDL analyzed by dynamic light scattering *via* a Zetasizer; (D) morphology and particle size of DMPC liposome and ApoE3−rHDL under a transmission electron microscope after negative staining with sodium phosphotungstate solution (1.75%, w/v), scale bar, 20 nm; (E) morphology and particle size of ApoE3−rHDL under atom force microscopy.

TABLE 1. Particle Size and Zeta Potential of Apolipoprotein E3−Reconstituted High Density Lipoprotein (ApoE3−rHDL)[a]

	particle size (nm)	polydispersity index	zeta potential (mV) at pH 7.4	zeta potential (mV) at pH 4.0
ApoE3−rHDL	27.9 ± 8.9	0.30	−4.07 ± 0.83	33.57 ± 0.55
DiI-labeled ApoE3−rHDL	21.7 ± 7.9	0.29	−2.55 ± 1.75	34.93 ± 2.40
^{125}I-labeled ApoE3−rHDL	21.6 ± 5.3	0.21	−5.39 ± 2.63	−

[a] DiI, 1,1′-dioctadecyl-3,3,3′,3′-tetramethylindocarbocyanine perchlorate; −, not determined.

binding, APOE ε2 allele individuals have a higher predisposition to diseases related to high amounts of cholesterol and triglycerides, and APOE ε4/ε4 homozygotic individuals have higher risk for coronary heart disease and a significantly greater risk for developing AD. Full-length recombinant ApoE3 was used here as the C-terminal domain (sequence 272−299) of ApoE is related to lipid binding and interaction with Aβ,[21] while the N-terminal domain (sequence 130−155) is responsible for low-density lipoprotein receptor (LDLR)/low-density lipoprotein receptor-related protein 1 (LRP1) binding that plays an important role in receptor-mediated endocytosis.[22,23]

ApoE is one of the best characterized apolipoproteins in structural term. It contains a series of amphipathic α-helical repeats, possesses detergent-like property and can solubilize vesicular phospholipids to create discoidal HDL particles.[24] Here the autoassemble reconstitution between DMPC liposome and ApoE3 was reflected by the change of 280 nm absorption of DMPC liposome in the presence of ApoE3 (Figure 1A). The density of the obtained ApoE3−rHDL (1.06−1.12 g/mL) was in the range of nature HDL (1.063−1.21 g/mL) (Figure 1B). Dynamic light scattering (DLS) (Figure 1C and Table 1), transmission electron microscopy (TEM) (Figure 1D) and atom force microscopy (AFM) (Figure 1E) were used for ApoE3−rHDL characterization. It was found that after the probe ultrasound treatment, small DMPC liposome (particle size 33.36 ± 11.04 nm, zeta potential −1.81 ± 0.20 mV) was obtained; following the incubation with ApoE3, nanodiscs with smaller size (27.94 ± 8.9 nm) and lower zeta potential (−4.07 ± 0.83 mV) at physiological pH were achieved. Fluorescent and radio-labeling did not change either the size or the zeta potential of ApoE3−rHDL (Table 1). The formation of nanodiscs was consistent with those rHDL reported previously using N-terminal of ApoE3, ApoA I or ApoA I mimetic peptide as the apolipoprotein component.[19,25−27] The obtained ApoE3−rHDL was also structurally similar with natural nascent HDL, and this lipidization process and the formation of nanodiscs is important as it can improve the affinity of ApoE to both its receptors and Aβ.[24,28−30] Compared with previous reported liposome decorated with ApoE or its derivative which did not include a direct interaction between the phospholipids

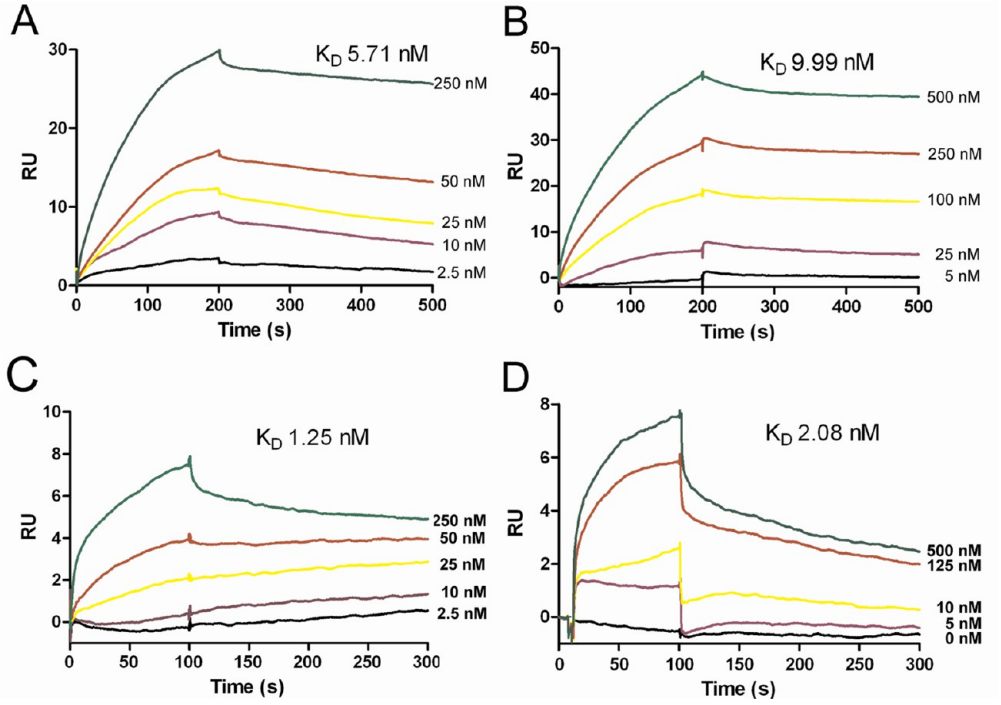

Figure 2. Concentration-dependent binding of apolipoprotein E3-reconstituted high density lipoprotein (ApoE3−rHDL) to Aβ monomers and oligomers, as evaluated by surface plasmon resonance analysis. Aβ monomer and oligomer were immobilized onto the surface of a CM5 sensor chip, separately, *via* an amine coupling reaction. Series concentration of ApoE3−rHDL was injected into the flow system, and the kinetic constants of binding were obtained using 1:1 Langmuir binding model *via* a BIAevaluation software. (A) Aβ_{1-40} monomer; (B) Aβ_{1-40} oligomer; (C) Aβ_{1-42} monomer; (D) Aβ_{1-42} oligomer.

TABLE 2. Average Affinity Constants Obtained from the Interaction between Apolipoprotein E3−Reconstituted High Density Lipoprotein (ApoE3−rHDL) and Aβ, $n = 3$[a]

immobilized protein	k_{ass} (M^{-1} s^{-1})	k_{diss} (s^{-1})	K_D (M)
Aβ_{1-40} monomer	$(8.39 \pm 0.45) \times 10^4$	$(4.93 \pm 0.08) \times 10^{-4}$	$(5.88 \pm 0.41) \times 10^{-9}$
Aβ_{1-40} oligomer	$(9.62 \pm 6.72) \times 10^4$	$(2.31 \pm 0.43) \times 10^{-4}$	$(4.58 \pm 4.73) \times 10^{-9}$
Aβ_{1-42} monomer	$(3.64 \pm 1.53) \times 10^5$	$(6.95 \pm 2.20) \times 10^{-4}$	$(2.32 \pm 1.71) \times 10^{-9}$
Aβ_{1-42} oligomer	$(3.30 \pm 2.54) \times 10^5$	$(11.97 \pm 6.65) \times 10^{-4}$	$(4.84 \pm 2.46) \times 10^{-9}$

[a] k_{ass}, association rate constant; k_{diss}, dissociation rate constant; and K_D, binding affinity constant.

membrane and ApoE,[31,32] the present biomimetic ApoE3−rHDL might provide several advantages such as smaller size, higher BBB-penetration efficiency and higher Aβ binding affinity.

ApoE3−rHDL Binds to Aβ Monomer and Oligomer with High Affinity. Aβ_{1-40} and Aβ_{1-42} are the most common sequential proteolytic byproducts of APP. Both of them form oligomers and protofibrils and have been found in amyloid plaques. Aβ_{1-40} constitutes about 90% of the most abundant cleaved form of APP, approximately 10-fold of Aβ_{1-42}. On the other hand, Aβ_{1-42} exhibits a greater propensity to aggregate than Aβ_{1-40} and it is the predominant and early component of AD plaques.[33] Here, the binding affinity of ApoE3−rHDL to the soluble forms of Aβ (both Aβ_{1-40} and Aβ_{1-42} monomer and oligomer) was determined *via* surface plasmon resonance (SPR) analysis. Aβ monomer and oligomer was immobilized onto the surface of a CM5 sensor chip, respectively, *via* an amine coupling reaction. Blank surface which was blocked with ethanolamine right after activation was used as reference. Kinetic analysis was performed to determine the rate of complex formation and dissociation. A low immobilization level (0.5−2 ng/mm^2, 500−2000 RU) was set to ensure the best performance of kinetic measurements. A concentration-dependent binding was recorded following the application of ApoE3−rHDL (Figure 2). By using 1:1 Langmuir binding model, the binding affinity constant (K_D) values obtained by ApoE3−rHDL were in the same nanomolar range as those of the nature derived ApoE3−rHDL (Table 2).[28] In contrast, ApoE3 alone exhibited a lower binding affinity to both Aβ_{1-40} and Aβ_{1-42} monomer (K_D 3.06×10^{-8} and 2.05×10^{-8} M, respectively).

TEM was here applied to reveal the Aβ oligomer-binding site on ApoE3−rHDL. Previous putative model suggested that in ApoE−HDL, ApoE circumscribe the periphery of a bilayer of phospholipids.[24] Under TEM,

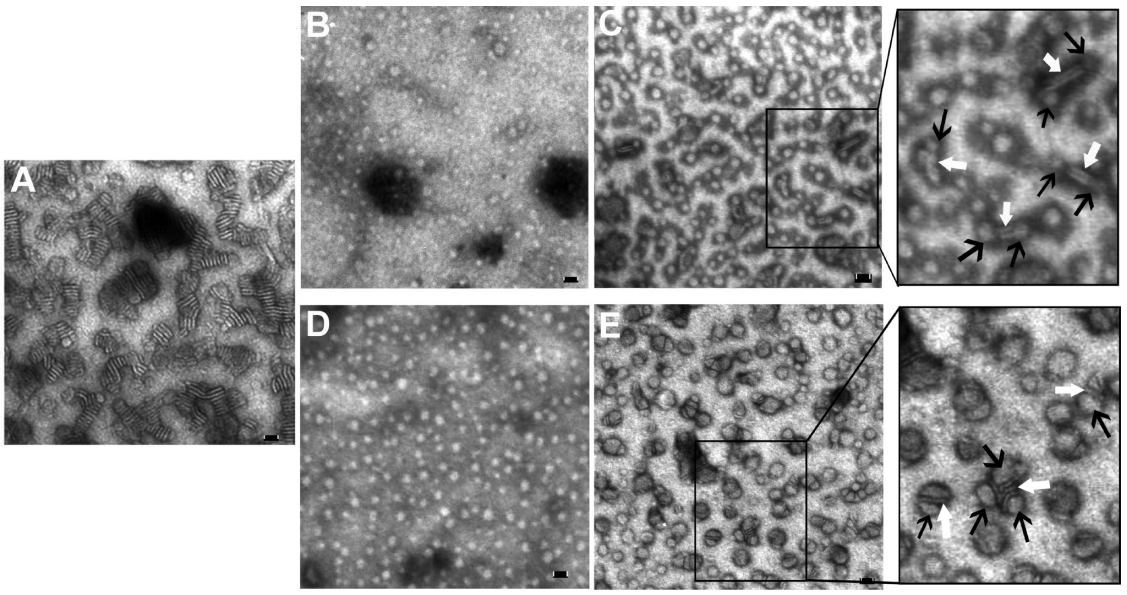

Figure 3. Interaction between apolipoprotein E3-reconstituted high density lipoprotein (ApoE3−rHDL) and Aβ oligomers monitored by transmission electrical microscopy (TEM): (A) ApoE3−rHDL; (B) Aβ_{1-40} oligomer; (C) Aβ_{1-40} oligomer (50 μM) incubated with ApoE3−rHDL (containing 250 μg/mL lipid) for 24 h; (D) Aβ_{1-42} oligomer; and (E) Aβ_{1-42} oligomer (50 μM) incubated with ApoE3−rHDL (containing 250 μg/mL lipid) for 24 h. The samples were negatively stained with 1.75% phosphotungstic acid before the TEM analysis. Scale bar, 20 nm. Black and white arrows in the zoom-in figures indicate Aβ oligomer and ApoE3−rHDL, respectively.

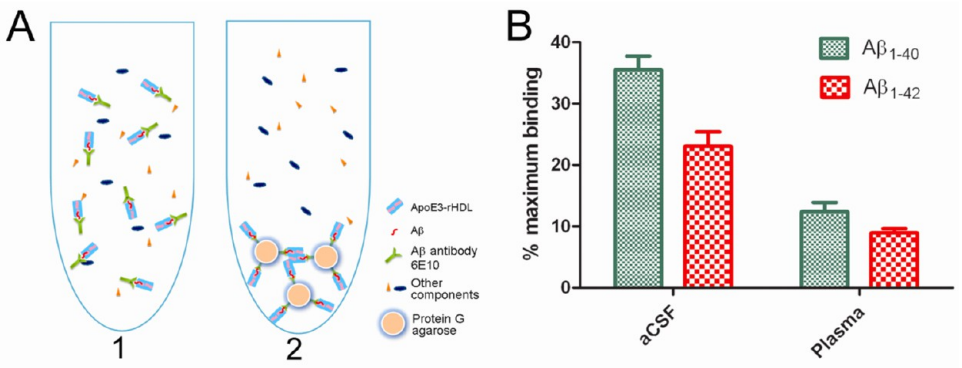

Figure 4. Co-immunoprecipitation analysis of the interaction between Aβ and apolipoprotein E3-reconstituted high density lipoprotein (ApoE3−rHDL). (A) Scheme shows ApoE3−rHDL co-immunoprecipitated by protein G agarose *via* the Aβ antibody 6E10:Aβ:ApoE3−rHDL interaction: 1, in the absence of protein G agarose; 2, in the presence of protein G agarose. (B) Percentage of 1,1′-dioctadecyl-3,3,3′,3′-tetramethylindocarbocyanine perchlorate (DiI)-labeled ApoE3−rHDL pulled down by protein G agarose in aCSF and plasma in the presence of Aβ antibody 6E10 and Aβ_{1-40} and Aβ_{1-42}, respectively. Using a 1:1:1 (6E10:Aβ:ApoE3−rHDL) binding model, the theoretical maximum amount of DiI-labeled ApoE3−rHDL that can be pulled down was calculated based on the hypothesis of 100% binding between 6E10 and protein G, between Aβ and the captured 6E10, and between ApoE3−rHDL and the captured Aβ. The amount of DiI-labeled ApoE3−rHDL pulled down was quantified *via* a fluorescence analysis at Ex 522 nm and Em 560 nm and expressed as % to the theoretical maximum binding. The treatment without the addition of Aβ was used as the negative control (zero control).

Aβ_{1-40} oligomer was found to bind to the lateral of ApoE3−rHDL nanodisc (Figure 3C); therefore, ApoE3 was believed to be the major binding site for Aβ_{1-40} oligomer. In the case of Aβ_{1-42} oligomer, it was also found to bind to or even fused with the nanodisc and form bigger nanostructure (Figure 3E). Such evidence suggested that ApoE3−rHDL might also serve as a useful nanocarrier for carrying therapeutic agents that can dissociate Aβ oligomer or help the clearance of Aβ.

Co-immunoprecipitation was performed to see if ApoE3−rHDL can bind to Aβ under physiological conditions (Figure 4). Artificial cerebrospinal fluid (aCSF) and mouse plasma were used as the binding media, respectively. Anti-Aβ antibody -6E10 was applied as the bait protein to see if ApoE3−rHDL can be captured *via* the Aβ:ApoE3−rHDL interaction. 1,1′-Dioctadecyl-3,3,3′,3′-tetramethylindocarbocyanine perchlorate (DiI) (2% to DMPC, w/w) was incorporated into the membrane of ApoE3−rHDL for fluorescent labeling, and the amount of DiI-labeled ApoE3−rHDL pulled down was quantified *via* a fluorescence analysis at Ex 522 nm and Em 560 nm. Using a 1:1:1 (6E10:Aβ:

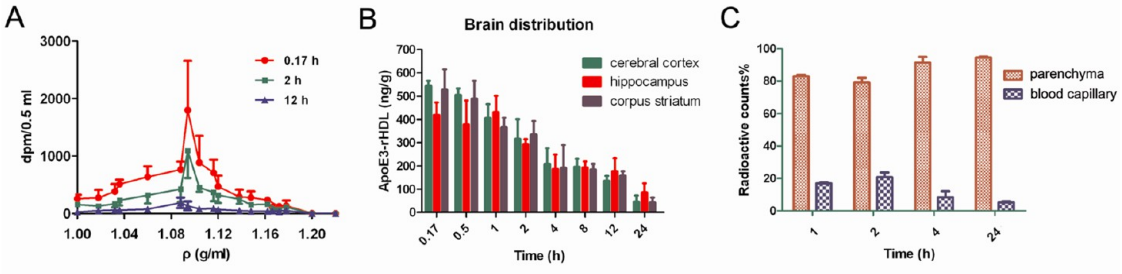

Figure 5. (A) Radioactivity in the brain homogenate at different density fractions after ultracentrifugation at 0.17, 2, and 12 h after intravenous administration of ^{125}I-ApoE3−rHDL. (B) Brain distribution of ^{125}I-ApoE3−rHDL at 0.17, 0.5, 1, 2, 4, 8, 12, and 24 h after intravenous administration. (C) Percentage of ^{125}I-ApoE3−rHDL accessing the brain parenchyma compared with that remained in the brain blood capillary at 1, 2, 4, and 24 h after intravenous administration.

ApoE3−rHDL) binding model, the theoretical maximum amount of ApoE3−rHDL that can be pulled down was calculated based on the hypothesis of 100% binding between 6E10 and protein G, between Aβ and the captured 6E10, and between ApoE3−rHDL and the captured Aβ. Using the treatment without the addition of Aβ as the negative control (zero control), after 3 h incubation at room temperature, we found ApoE3−rHDL to be effectively pulled down by protein G agarose in both aCSF (35.50 ± 3.82 and 23.00 ± 4.12% accounting to the maximum theoretical binding) and plasma (12.40 ± 2.65 and 8.96 ± 1.19% accounting to the maximum theoretical binding) in the presence of Aβ_{1-40} and Aβ_{1-42}, respectively. Compared with aCSF, the plasma contains higher concentration of proteins including native HDL that can also bind to Aβ; therefore, it is no surprise to see higher binding in aCSF. Considering that the binding between 6E10 and protein G, and that between Aβ and 6E10 captured by protein G can hardly achieve 100%, these data strongly indicated that ApoE3−rHDL can effectively bind to Aβ under physiological conditions.

Brain Distribution of ApoE3−rHDL Following Intravenous Administration. Accessing the brain is one of the major prerequisites for ApoE3−rHDL to mediate intracerebral Aβ degradation. The expression of receptors to ApoE, LDLR and LRP1, was found on the BBB. Previous work has witnessed the transcytosis of LDL and ApoE-modified albumin nanoparticles across the BBB *via* a receptor-mediated process.[18] Therefore, ApoE3−rHDL, which possesses higher binding affinity to these receptors and much smaller particle size, is expected to exhibit more efficient BBB permeability. To evaluate the brain delivery efficiency, ApoE3−rHDL was here labeled with ^{125}I *via* the Bolton-Hunter procedure,[34] and its biodistribution following intravenous administration was determined *via* a γ-counter and expressed as percentage injected dose per gram tissue (% ID/g). As a control, biodistribution of ^{125}I-labeled ApoE3 (^{125}I-ApoE3) was also analyzed. As shown in Supporting Information Figure S1, lipidization of ApoE3 changed the biodistribution behavior of ApoE3 in the heart, liver and kidney. In the case of brain distribution, radioactivity detected in the brain after intravenous administration of ^{125}I-labeled ApoE3−rHDL (^{125}I-ApoE3−rHDL) was comparable with that of ^{125}I-ApoE3 at the early time points (0.17 and 0.5 h), but higher than that of ^{125}I-ApoE3 at the later time points (from 1 to 24 h), suggesting that the clearance of ^{125}I-ApoE3−rHDL from the brain might be slower than that of ^{125}I-ApoE3.

After correction for *ex vivo* degradation by acid precipitation, 83.92 ± 13.21%, 80.29 ± 8.84%, and 67.23 ± 20.87% of the total brain radioactivity were found precipitated at 0.17, 2, and 12 h following intravenous administration of ^{125}I-ApoE3−rHDL, respectively, indicating that the radiolabeling is quite stable. To tell if the radioactivity represent intact ^{125}I-ApoE3−rHDL that delivered into the brain, ultracentrifugation was performed with different density sections of the brain homogenate subjected to radioactivity assay. It was found that most of the brain radioactivity was detected at the density fraction between 1.06 and 1.12 g/mL (Figure 5A), which was within the density range of nature HDL (1.063−1.21 g/mL), suggesting that most of the radioactivity might represent intact ^{125}I-ApoE3−rHDL. One hour after administration, the amount of ^{125}I-ApoE3−rHDL accumulated in the cerebral cortex, hippocampus and corpus striatum was 407.01 ± 58.30 ng/g (0.41 ± 0.06% ID/g), 430.11 ± 71.85 ng/g (0.43 ± 0.07% ID/g), and 366.09 ± 41.31 ng/g (0.37 ± 0.04% ID/g), respectively (Figure 5B). Such brain delivery efficiency was comparable with that of the well-acknowledged nanocarriers for brain-targeting drug delivery (OX26 immunoliposome,[35] lactoferrin-functionalized polyamidoamine[36] and polysorbate 80-coated poly-(*n*-butyl cyanoacrylate) nanoparticles[37]) but lower than that of the receptor for advanced glycation end products (RAGE)-mediated blood-to-brain Aβ transport.[38] As ApoE3−rHDL also exhibited considerable binding affinity to circulating Aβ, such lower BBB-penetrating effeciency of ApoE3−rHDL compared with Aβ would step down rather than facilitate the transport of Aβ into the brain.

Capillary depletion technique was employed to distinguish between the amounts of ^{125}I-ApoE3−rHDL in the whole brain and that in the brain parenchyma

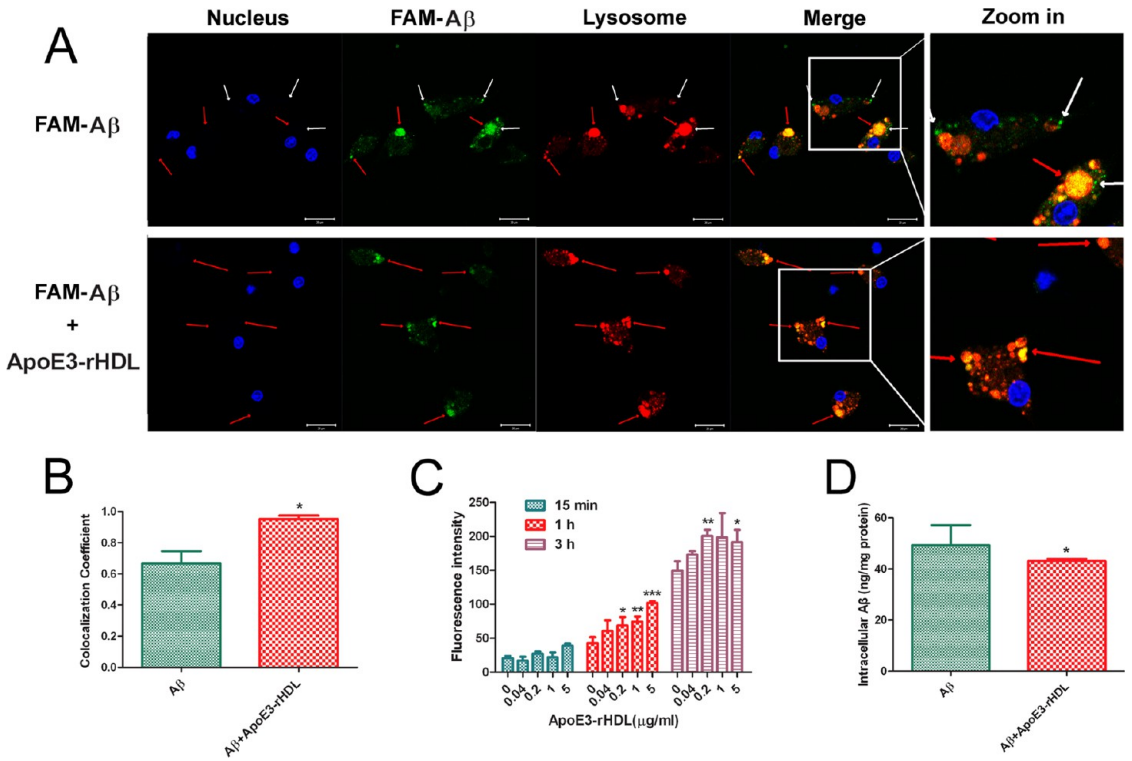

Figure 6. Effect of ApoE3−rHDL on the microglia cellular uptake, intracellular distribution and degradation of $A\beta_{1-42}$. (A) Cellular uptake and distribution of FAM-labeled $A\beta_{1-42}$ (FAM-Aβ) in primary microglia in the absence or presence of ApoE3−rHDL (1 μg/mL) after incubation for 15 min. Lysosome was indicated by LysoTracker Red. Red arrow, FAM-Aβ colocalized with lysosome; white arrow, FAM-Aβ did not colocalize with lysosome; scale bar: 20 μm. (B) Colocalization coefficient of FAM-Aβ to lysosome, $n = 7$.(C) Cellular uptake of FAM-Aβ in primary microglia in the presence of ApoE3−rHDL (0, 0.04, 0.2, 1, and 5 μg/mL) after incubation for 15 min, 1 h and 3 h, respectively. (D) Intracellular $A\beta_{1-42}$ levels were quantified by ELISA and normalized to total protein ($n = 3$) after 3 h of incubation with Aβ only or Aβ+ApoE3−rHDL at the ApoE3−rHDL concentration of 1 μg/mL. *$p < 0.05$, **$p < 0.01$, ***$p < 0.001$ significantly different with that of those treated with Aβ only.

after crossing the BBB.[37,39] It was found that 1 h following injection, more than 80% of the brain ^{125}I-ApoE3−rHDL accumulated in the parenchyma. This percentage increased to 94.6 ± 1.1% at 24 h after administration (Figure 5C). These evidence strongly suggested that ApoE3−rHDL could be effectively transported from the blood circulation into the brain parenchyma. Although the distribution of ApoE3−rHDL in the brain is far less than that in the peripheral organs, as the vasculature system is extensively distributed in the CNS and every neuron is perfused by its own blood vessel, transvascular route of drug administration, following intravenous injection, could be delivered to all parts of the brain once the vascular barrier is traversed.[40] *In vitro* co-immunoprecipitation analysis with lower mass ratio between ApoE3−rHDL and Aβ (225 and 10 μg/mL, respectively) showed effective binding between ApoE3−rHDL and Aβ. Therefore, we believed that in real biological system, where the mass ratio between ApoE3−rHDL (about 400 ng/g) and Aβ (low ng/mL) is much higher,[41,42] Aβ could be more effectively captured by ApoE3−rHDL. Considering that rHDL is a versatile class of biologically inspired nanostructures that can carry both hydrophobic and hydrophilic agents,[43] ApoE3−rHDL might also serve as a nanocarrier for brain drug delivery especially for the treatment of AD.

ApoE3−rHDL Accelerates Microglial and Astroglial Degradation of Aβ. Microglial and astroglial uptake and degradation is one of the key mechanisms for brain Aβ clearance.[44−46] Previous work showed that lipidated ApoE promoted microglia and astrocyte-mediated Aβ degradation.[45,46] In this work, a high binding affinity was observed between Aβ and ApoE3−rHDL in the aCSF. To evaluate the effect of ApoE3−rHDL on intracerebral Aβ degradation, primary microglia and astrocytes were cultured as described previously,[46] and incubated with soluble $A\beta_{1-42}$ in the presence of ApoE3−rHDL with the cellular uptake, intracellular distribution and degradation of $A\beta_{1-42}$ evaluated. High content screening (HCS), a cell-based quantitative fluorescence imaging system,[47] was applied to quantitatively determine the cellular uptake of Aβ in the presence of ApoE3−rHDL. As shown in Figures 6C and 7C, the cellular uptake of Aβ did not change after a short incubation time (*e.g.*, 15 min), but increased 1 and 3 h after co-incubation with ApoE3−rHDL. As both microglia and astrocytes also expressed low density lipoprotein receptor-related protein that can capture Aβ, it was no surprise to see efficient internalization of

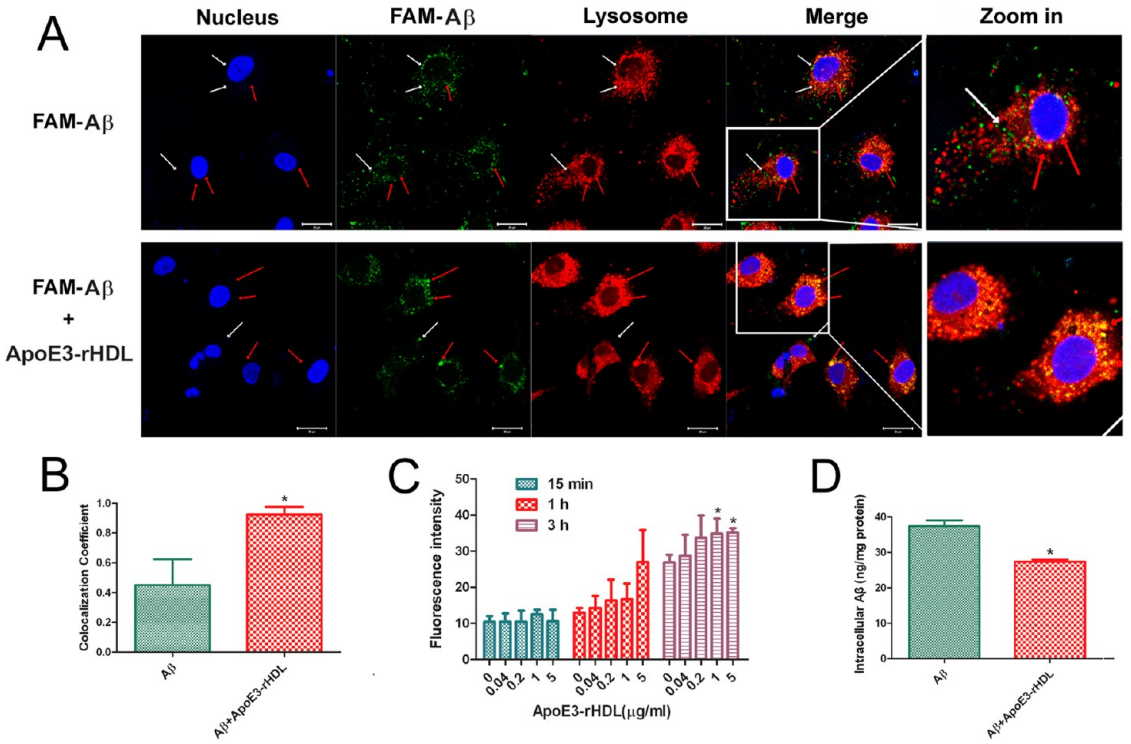

Figure 7. Effect of ApoE3−rHDL on the astrocytes cellular uptake, intracellular distribution and degradation of $A\beta_{1-42}$. (A) Cellular uptake and distribution of FAM-labeled $A\beta_{1-42}$ (FAM-Aβ) in primary astrocytes in the absence or presence of ApoE3−rHDL (1 μg/mL) after incubation for 15 min. Lysosome was indicated by LysoTracker Red. Red arrow, FAM-Aβ colocalized with lysosome; white arrow, FAM-Aβ did not colocalize with lysosome; scale bar: 20 μm. (B) Colocalization coefficient of FAM-Aβ to lysosome, $n = 7$. (C) Cellular uptake of FAM-Aβ in primary astrocytes in the presence of ApoE3−rHDL (0, 0.04, 0.2, 1, and 5 μg/mL) after incubation for 15 min, 1 h and 3 h, respectively. (D) Intracellular $A\beta_{1-42}$ levels were quantified by ELISA and normalized to total protein ($n = 3$) after 3 h of incubation with Aβ only or Aβ+ApoE3−rHDL at the ApoE3−rHDL concentration of 0.2 μg/mL. *$p < 0.05$, significantly different with that of those treated with Aβ only.

Aβ by these cells in the absence of ApoE3−rHDL. However, the important phenomenon we found is that even with no difference in the total amount of Aβ internalized after a short time incubation (15 min), the colocalization of Aβ with lysosome was significantly increased in the presence of ApoE3−rHDL (Figures 6A, B, and 7A,B), suggesting that ApoE3−rHDL could facilitate the lysosomal transport of Aβ. As a result, even with higher amount of Aβ internalized into the cells after a longer incubation (3 h) (Figures 6C and 7C), the intracellular Aβ detected by ELISA in those Aβ+ApoE3−rHDL-treated cells was still significantly lower than that in the Aβ only-treated controls (Figure 6D and 7D). These evidence collectively strongly indicated that the intracellular degradation of Aβ was accelerated in the presence of ApoE3−rHDL in both microglia and astrocytes.

ApoE3−rHDL Promotes Liver Cellular Uptake and Clearance of Aβ. Liver has been claimed to be the major organ for peripheral Aβ degradation and clearance.[10,48] Biodistribution analysis showed that liver was also the major organ where ApoE3−rHDL accumulated (Supporting Information Figure S1). Therefore, the effect of ApoE3−rHDL on liver cellular uptake and clearance of Aβ was also evaluated here. Using Chang liver cells as the cell model, we found that similar with that in both microglia and astrocytes, the cellular uptake of Aβ was enhanced in the presence of ApoE3−rHDL after incubation for 3 h (Figure 8C). In addition, more Aβ was found colocalized with lysosome (Figure 8A,B). As a result, after 3 h of incubation, more Aβ was degraded in the presence of ApoE3−rHDL (Figure 8D). Considering that the ApoE3−rHDL developed here also exhibited considerable binding affinity to both $A\beta_{1-40}$ and $A\beta_{1-42}$ in plasma, we believed that those ApoE3−rHDL did not cross the BBB and might also bind to Aβ in the circulation and redirect the peptide to the liver for degradation.

ApoE3−rHDL Decreases Amyloid Deposition, Attenuates Microgliosis, Ameliorates Neurologic Changes, and Rescues Memory Deficits in AD Model Mice. To evaluate the disease-modifying effects of ApoE3−rHDL in AD, the senescence-accelerated prone mouse (SAMP8), which exhibits age-related cognitive decline with relevance to alterations of the gene expression and protein abnormalities in AD, was used as the AD animal model.[49] The age-matched strain senescence-accelerated mouse resistant R1 (SAMR1) was used as the normal control. Anti-Aβ immunostaining demonstrated that amyloid plaque loads in both the cortex and hippocampus were markedly decreased in the ApoE3−rHDL-treated SAMP8 mice when compared with the saline-treated ones (40% and 64% of decrease, respectively) (Figure 9A,C).

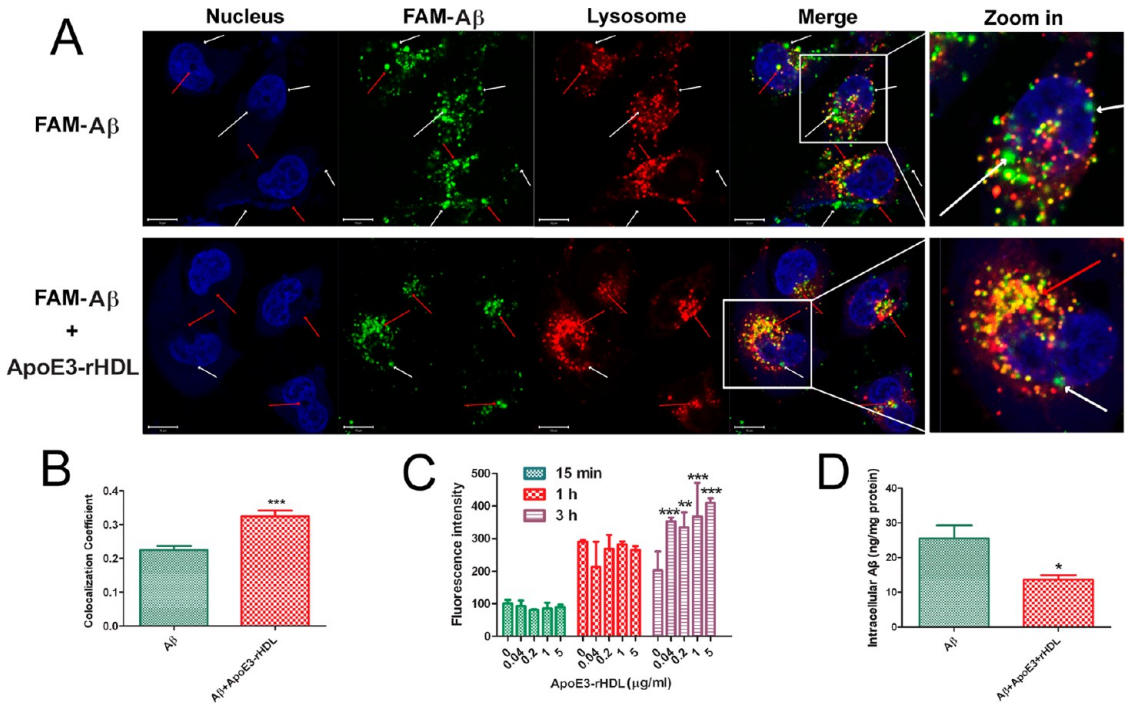

Figure 8. Effect of ApoE3−rHDL on the Chang liver cellular uptake, intracellular transport and degradation of $A\beta_{1-42}$. (A) Cellular uptake and distribution of FAM-labeled $A\beta_{1-42}$ (FAM-Aβ) (green) in Chang liver cells in the absence or presence of ApoE3−rHDL (1 μg/mL) after incubation for 3 h. Lysosome was indicated by LysoTracker Red. Red arrow, FAM-Aβ colocalized with lysosome; white arrow, FAM-Aβ did not colocalize with lysosome; scale bar, 10 μm. (B) Colocalization coefficient of FAM-Aβ to lysosome, $n = 7$. (C) Cellular uptake of FAM-Aβ in Chang liver cells in the presence of ApoE3−rHDL (0, 0.04, 0.2, 1, and 5 μg/mL) after incubation for 15 min, 1 h and 3 h, respectively. (D) Intracellular $A\beta_{1-42}$ levels were quantified by ELISA and normalized to total protein ($n = 3$) after 3 h of incubation with Aβ only or Aβ+ApoE3−rHDL at the ApoE3−rHDL concentration of 5 μg/mL. *$p < 0.05$, **$p < 0.01$, ***$p < 0.001$, significantly different with that of those treated with Aβ only.

Abnormal activation of microglia is observed in the brains of AD patients and mouse models of amyloidosis.[50] Previous studies suggested that both Aβ oligomers and fibrils triggered neuroinflammatory cascades.[51] We here assessed the activation of microglia by using CD45 as the markers. Compared with that in the saline-treated SAMP8 mice, approximately an 80% decrease in the CD45-positive activated microglial load was achieved in the ApoE3−rHDL-treated animals (Figure 9B,D). Given the central role of Aβ aggregates in the activation of microglia seen in AD brain, the significant decrease in activated microglia seen in the ApoE3−rHDL-treated mice could be attributed to the activity of ApoE3−rHDL in facilitating Aβ clearance.

Neuronal loss in the cortex and hippocampus is one of the key hallmarks of AD.[52] Nissl staining and hematoxylin/eosin (HE) staining analysis showed that compared with that in the SAMR1 mice, neuronal hypocellularity and neuron nuclear shrinkage were observed in both the cortex and hippocampus of the saline-treated SAMP8 mice. In contrast, ApoE3−rHDL treatment significantly attenuated impairment of neuronal integrity and neuron loss in SAMP8 mice (Figure 10).

The spatial learning and memory were assessed *via* a Morris water maze test in 7-month-old SAMP8 mice after a four-week daily treatment of ApoE3−rHDL (containing DMPC 5 mg/kg, ApoE3 1 mg/kg) using SAMR1 mice as the normal control. SAMP8 mice treated with saline was applied as the negative control, and showed deficits in their learning performance compared with SAMR1 mice. In contrast, ApoE3−rHDL-treated SAMP8 mice exhibited significantly improved spatial learning and memory on the measures of water maze performance, both escape latency and swimming speed (Figure 11A,B) during the four-day training process. After removing the escape platform, SAMR1 mice concentrated searches for the platform in the quadrant where it used to be located, whereas saline-treated SAMP8 mice exhibited poorly focused search strategies (Figure 11). After the ApoE3−rHDL treatment, SAMP8 mice showed marked improvement in searching strategy, with significantly longer swimming time spend around the platform location (Figure 11).

After the four-week daily treatment with ApoE3−rHDL at the DMPC dose of 5 mg/kg, the animals were sacrificed with the major organs collected for HE staining to evaluate the biosafety of ApoE3−rHDL for AD therapy. No obvious microscopic alterations were observed in the hearts, livers, spleens and kidneys of the ApoE3−rHDL-treated animals compared with the saline-treated ones. In the case of the lung, as

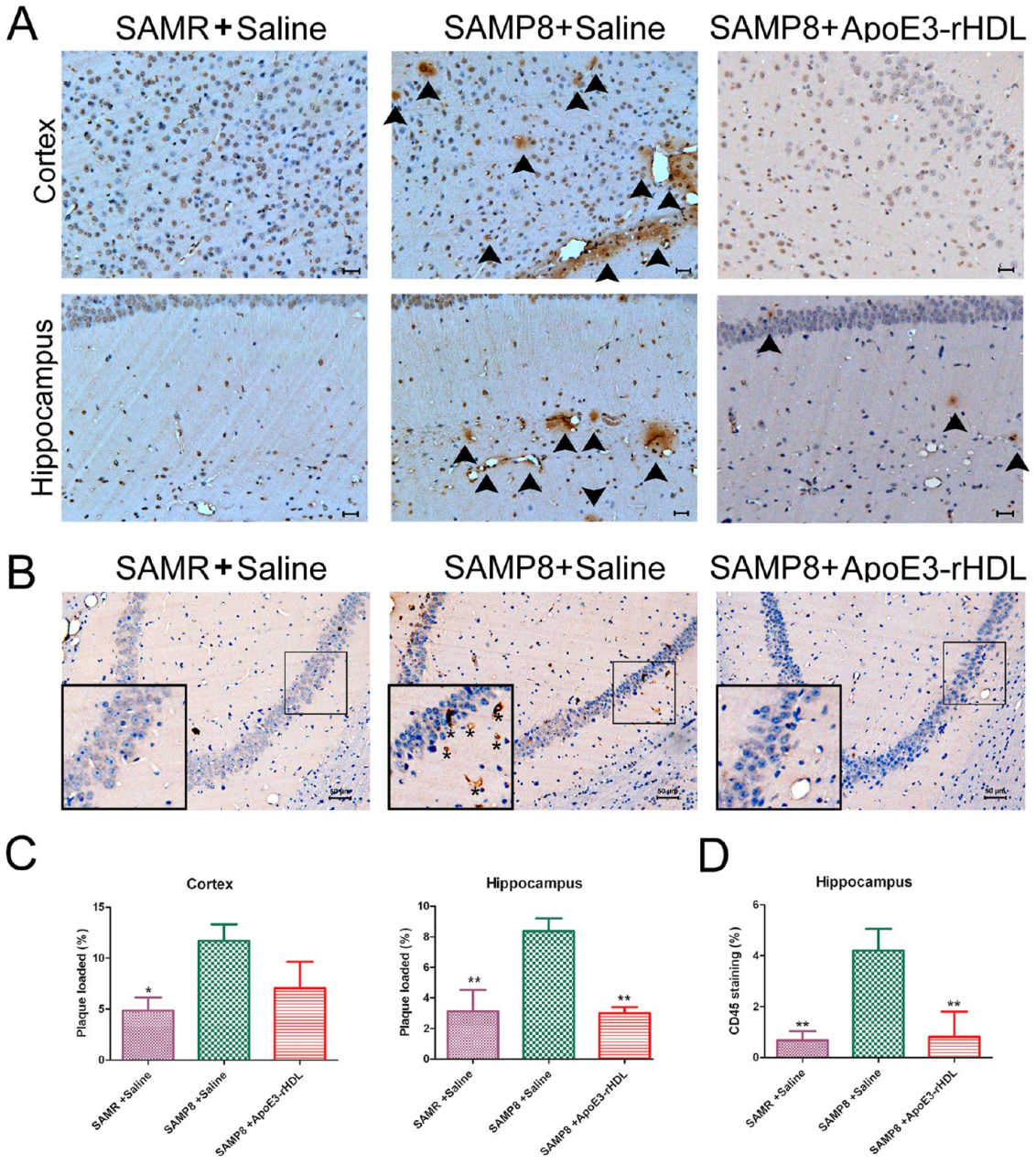

Figure 9. ApoE3−rHDL decreased amyloid deposition (brown signals as indicated by arrowhead) (A and C) and attenuated microgliosis (brown signals as indicated by star in the zoom graphs) (B and D) in SAMP8 mice. Seven-month-old SAMP8 mice (n = 8−9 per group) were treated with ApoE3−rHDL at the DMPC dose of 5 mg/kg intravenously *via* the tail vein daily for 4 weeks with the age-matched SAMP8 and SAMR1 mice given with saline as the negative and normal control, respectively. Brain sections (3 μm) were immunostained with anti-Aβ antibody 6E10 and anti-CD45 antibody, respectively. *$p < 0.05$, **$p < 0.01$ significantly different with that of the saline-treated SAMP8 mice.

mentioned in previous reports,[53] inflammatory responses such as interalveolar septum hemorrhage, perialveolar capillary hyperemia, and interstitial focal lymphocytic infiltration were observed in the saline-treated SAMP8 mice. Interestingly, such pathologic changes were not seen in the ApoE3−rHDL-treated animals (Supporting Information Figure S2). As HDL also possesses anti-inflammatory activity, we speculated that ApoE3−rHDL might alleviate the inflammatory response in the lungs of SAMP8 mice *via* the same mechanism. In the case of brain, as shown in Figures 9 and 10, ApoE3−rHDL treatment attenuated microgliosis and ameliorated neurologic changes in SAMP8 mice without causing other visible damage to the brain tissue. Collectively, these preliminary data suggested that, under our current dosing regimen, the *in vivo* application of ApoE3−rHDL might be safe. However, for anti-AD therapy, the long-term *in vivo* safety still needs to be further evaluated.

Taken together, four-week daily treatment with ApoE3−rHDL effectively decreased Aβ deposition, attenuated microgliosis, ameliorated neurologic changes

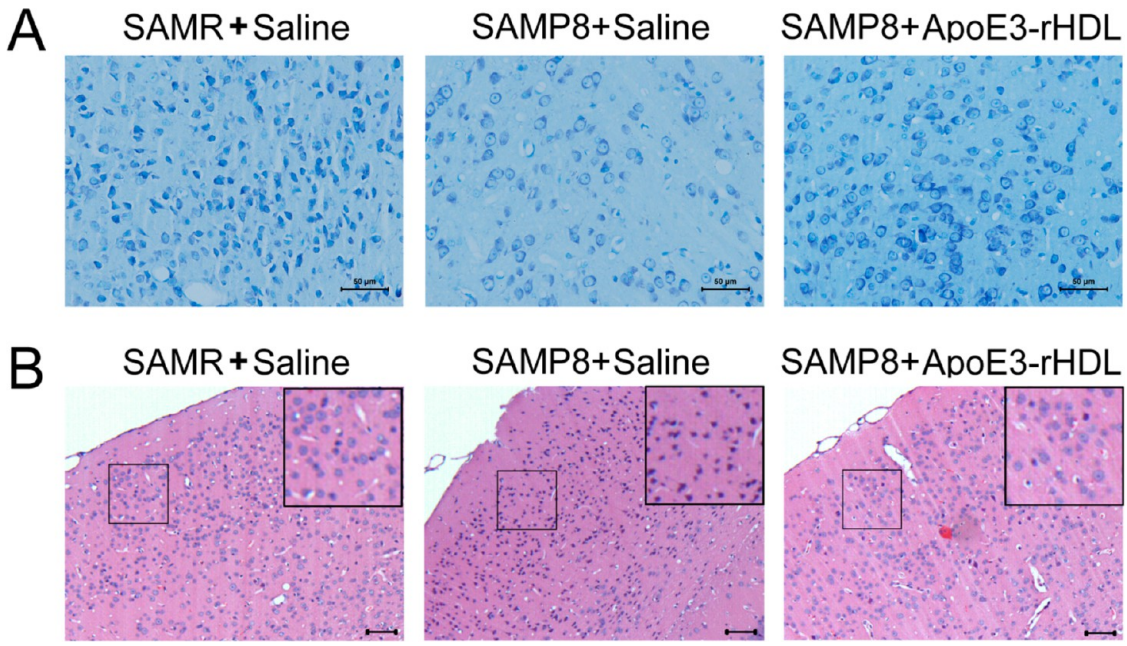

Figure 10. ApoE3−rHDL ameliorated neurologic changes (neuronal hypocellularity and neuron nuclear shrink) in SAMP8 mice. Seven-month-old SAMP8 mice (n = 8−9 per group) were treated with ApoE3−rHDL at the DMPC dose of 5 mg/kg intravenously *via* the tail vein daily for 4 weeks with the age-matched SAMP8 and SAMR1 mice given normal saline as the negative and normal control, respectively. The brain slices were stained with (A) Nissl or (B) hematoxylin/eosin following standard protocol. Scale bar, 50 μm.

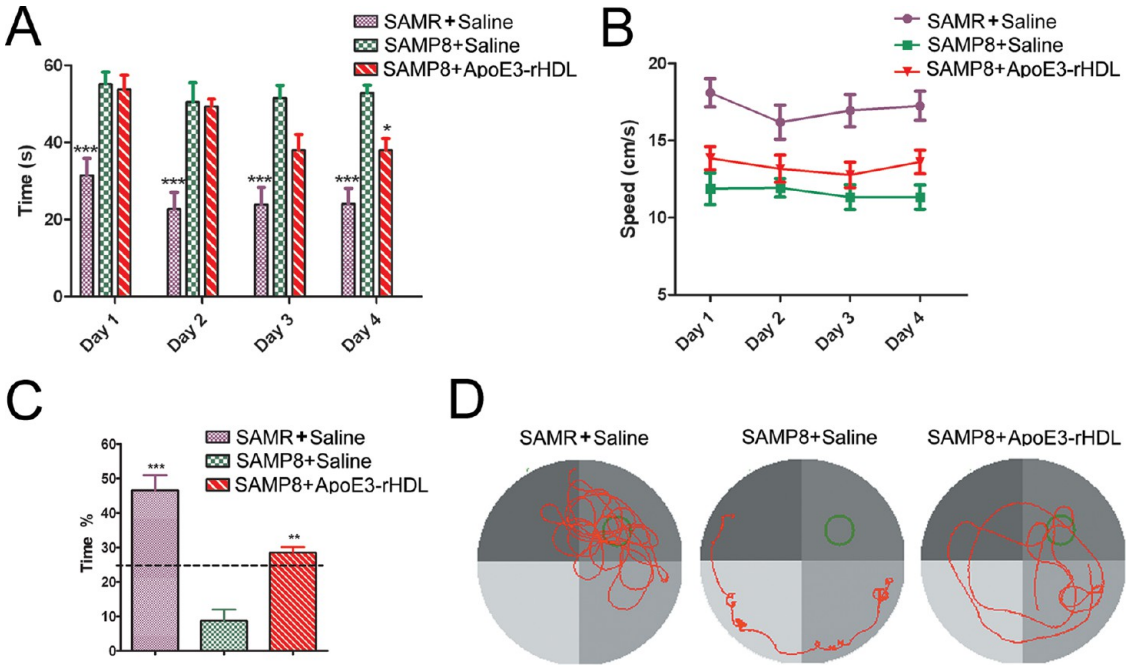

Figure 11. ApoE3−rHDL rescued memory deficits in SAMP8 mice. Seven-month-old SAMP8 mice (n = 8−9 per group) were treated with ApoE3−rHDL at the DMPC dose of 5 mg/kg intravenously *via* the tail vein daily for 4 weeks with the age-matched SAMP8 and SAMR1 mice given normal saline as the negative and normal control, respectively. (A) Escape latency; (B) swimming speed; (C) percentage of time spent in the quadrant where the escape platform used to located; (D) representative swimming path. Data represent mean ± SEM; *p < 0.05, **p < 0.01, ***p < 0.001 significantly different with those of the saline-treated SAMP8 mice.

and rescued memory deficits in SAMP8 mice. To our knowledge, this is the first evidence of a biomimetic nanostructure that exhibits disease-modifying effectiveness in AD clinically relevant biological systems. As rHDL is a versatile nanostructure that can also carry various agents, ApoE3−rHDL holds great potential in exerting synergistic effect with its payload for the treatment of AD.

CONCLUSIONS

In summary, a biologically inspired nanostructure, ApoE−rHDL, that with ApoE3, the most predominant ApoE isoform in healthy population, as the apolipoprotein component, was here designed as a novel nanomedicine by binding to Aβ with high affinity and accelerating its clearance. Both *in vitro* and *in vivo* experiments were performed to justify this possibility and the remarkable disease-modifying effects of this biomimetic nanomedicine were reported. It was found that the obtained ApoE3−rHDL demonstrated high binding affinity to both Aβ monomer and oligomer, and accelerated microglial, astroglial and liver cell degradation of Aβ by facilitating the lysosomal transport. More importantly, we found that following intravenous administration, part of ApoE3−rHDL gained access to the CNS. As a result, four-week daily administration of ApoE3−rHDL decreased amyloid deposition, attenuated microgliosis, ameliorated neurologic changes and rescued memory deficits in an AD animal model. The findings here provided the direct evidence of a biomimetic nanostructure crossing BBB, capturing Aβ and facilitating its degradation by glial cells, indicating that biologically inspired ApoE3−rHDL might serve as a novel nanomedicine for disease modification in AD by accelerating Aβ clearance, which also justified the concept that nanostructures with Aβ-binding affinity might provide a novel nanoplatform for AD therapy.

MATERIALS AND METHODS

Materials. DMPC was obtained from Avanti Polar Lipids, Inc. (Alabaster, AL). Full-length ApoE3 was provided by PEPROTECH, Inc. (Rocky Hill, NJ). Aβ_{1-40}, Aβ_{1-42} peptides, DiI, Aβ ELISA Kits and LysoTracker Red were purchased from Invitrogen (Carlsbad, CA). FAM-labeled Aβ_{1-42} (FAM-Aβ) was provided by AnaSpec, Inc. (Fremont, CA). Mouse monoclonal antibody 6E10 reactive to amino acid residues 1−16 of Aβ was obtained from Covance (Emeryville, CA) and purified anti-mouse CD45 antibody was from BD Biosciences (San Jose, CA). All the cell culture reagents were purchased from GIBCO (Grand Island, NY) unless otherwise indicated.

Cells. Primary microglial cells were derived from the brains of Sprague−Dawley (SD) rats at postnatal day 1−2 as previously described.[54] Cells were maintained in DMEM/F12 (Invitrogen) containing 1% penicillin/streptomycin and 20% fetal bovine serum (FBS), pH 7.4. Primary astrocytes were separated from the microglial cultures using a mild trypsinization protocol described by Saura *et al.*[55] Chang liver cells were obtained from ATCC and cultured at 37 °C in 5% CO_2 using the culture medium containing DMEM, 10% FBS, 1% L-glutamine, 1% penicillin−streptomycin solution and 1% nonessential amino acids.

Animals. SAMP8 and SAMR1 mice were provided by Animal center of the First Affiliated Hospital of Tianjin University of Traditional Chinese Medicine. SD rats and Kunming mice were obtained from Shanghai SLAC Laboratory Animal CO. LTD (Shanghai, China). The animals were housed in the specific pathogen-free animal facility with free access to food and water. The protocol of animal experiments was approved by the Animal Experimentation Ethics Committee of approved by the appropriate ethical committee of Shanghai Jiao Tong University School of Medicine.

Preparation and Characterization of ApoE3−rHDL. Four milligrams of DMPC was dissolved in chloroform and the solution was dried under a high vacuum at 30 °C using Büchi rotavapor R-200 (Büchi, Germany). The lipid film was then rehydrated in 4 mL of 0.01 M PBS buffer (pH 7.4) by vortexing intermittently for 5 min. The turbid emulsion was subsequently bath sonicated at 40 °C for 1 h and then probe sonicated (Scientz Biotechnology Co. Ltd., China) at 200 W output for 15 min. ApoE3 (0.8 mg) suspended in 2 mL of PBS buffer was added into the emulsion. The resulting mixture was further incubated at 37 °C for 36 h before subjection to purification by density gradient ultracentrifugation.

The morphology and size of ApoE3−rHDL was observed under a Hitachi H-7650 transmission electron microscope (Hitachi, Inc., Japan) after negative staining with 1.75% sodium phosphotungstate solution, and characterized *via* an atom force microscope (Dimension Icon, Bruker, German). The particle size distributions and zeta potential of ApoE3−rHDL were measured by photon correlation spectroscopy (Zetasizer Nano-ZS90, Malvern Instruments, U.K.) utilizing a 4.0 mW He−Ne laser operating at 633 nm and a detector angle of 90°.

Preparation of Aβ_{1-40} and Aβ_{1-42} Monomer and Oligomer. Aβ_{1-40} or Aβ_{1-42} was first dissolved in hexafluoroisopropanol (HFIP) at 1 mg/mL and stored at −20 °C. Before use, HFIP was allowed to evaporate, and the peptide was resuspended in dimethyl sulfoxide (DMSO) at the concentration of 5 mM and bath sonicated for 10 min to obtain the monomeric preparation. Aβ_{1-40} oligomer was prepared by diluting the monomeric peptide HFIP solutions to 230 μM with ddH_2O, evaporating the HFIP and incubating the solution at 22 °C for 48 h as described previously.[56] For the preparation of Aβ_{1-42} oligomer, monomeric peptide DMSO solution (5 mM) was diluted to 100 μM in 50 mM phosphate buffer containing 150 mM NaCl, pH 7.4, and incubated for 24 h at 4 °C.[57] The presence of oligomer in these preparations has been previously confirmed and characterized.[58]

SPR Analysis. Aβ_{1-40}/Aβ_{1-42} monomer and oligomer as prepared above were immobilized in parallel-flow channels of a CM5 sensor chip (GE) using the amine coupling reaction. Briefly, after surface activation with 0.2 M ethyl(dimethylaminopropyl)-carbodiimide (EDC) and 0.05 M *N*-hydroxysuccinimide (NHS), the peptide solutions (50 μM in acetate buffer pH 4.0) were injected to achieve a preset immobilization level (500−2000 RU, 0.5−2 ng/mm^2) with the remaining activated groups blocked with ethanolamine, pH 8.5. The upstream parallel flow cell, which was activated with EDC/NHS and then blocked by 1 M ethanolamine, was used as the control surface to normalize the SPR signals from the peptide-immobilized channel. Experiments were conducted with PBS (pH 7.4) as the running buffer, and the analyte was injected at the flow rate of 30 μL/min. Dissociation was followed for 8 min before the regeneration of the chip with 50 mM NaOH. Equilibration of the chip with the running buffer for another 8 min was performed before the next injection. Series concentration of ApoE3−rHDL or ApoE3 solutions (diluted in 0.01 M PBS, pH 7.4, containing 0−500 nM ApoE3) was injected into the flow system, and the kinetic constants of binding were obtained using 1:1 Langmuir binding model *via* a BIAevaluation software.

Co-immunoprecipitation Analysis. The specific binding of ApoE3−rHDL to Aβ_{1-40}/Aβ_{1-42} monomers in both aCSF and mouse plasma was also evaluated by a modified coimmunoprecipitation procedure. DiI (2% to DMPC, w/w) was incorporated in the membrane of ApoE3−rHDL for fluorescent labeling. For the analysis, ApoE3−rHDL 225 μg/mL and Aβ 10 μg/mL were first incubated at 4 °C overnight in the aCSF and mouse plasma, respectively, with anti-Aβ antibody 6E10 (20 μg/mL) applied as the bait protein to capture the Aβ:ApoE3−rHDL complex. Protein G agarose (100 μL) was then added for 6E10 binding. After 2 h of incubation, the pulled down 6E10:Aβ:ApoE3−rHDL complex was desorbed from the agarose and subjected to measurement of fluorescent intensity at the

excitation wavelength 522 nm and emission wavelength 560 nm for ApoE3−rHDL quantification. ApoE3−rHDL captured by protein G agarose in the absence of Aβ was used as the negative control (zero control).

Brain Distribution of ApoE−rHDL Following Intravenous Administration. ApoE3−rHDL and ApoE3 were radioactively labeled with ^{125}I *via* the Bolton-Hunter Procedure as described previously.[34] For biodistribution analysis, Kunming mice (20 ± 2 g) received a bolus of ^{125}I-ApoE3−rHDL (25 μCi/mouse in 300 μL, DMPC dose of 5 mg/kg) or ^{125}I-ApoE3 (25 μCi/mouse in 300 μL, ApoE3 dose of 1 mg/kg) *via* the tail vein. At designated time points (0.17, 0.5, 1, 2, 4, 8, 12, and 24 h after injection), blood was collected and the mouse was decapitated immediately with the brain cerebrum, hippocampus, thalamus, corpus striatum and peripheral tissue samples collected, weighed, and assayed for radioactivity. Aliquots of the blood and tissue samples were homogenized and precipitated in 6-fold weight of cold 10% trichloroacetic acid (TCA) for examining the metabolic stability of the labeling.

To determine if intact ^{125}I-ApoE3−rHDL was transported into the brain, ultracentrifugation in potassium bromide (KBr) solution was performed as described previously.[59] The brain tissue was homogenized in 3 vol of distilled water and diluted 10 times with KBr solution to the density of 1.063 g/mL. Before ultracentrifugation, 2 mL of the KBr solution of density 1.240 g/mL was added into the bottom of the tube. The following solutions were then layered onto the latter: 2 mL of KBr solution of density 1.21 g/mL, 2 mL of the diluted homogenate and 2 mL of NaCl solution of density 1.006 g/mL. Immediately upon completion, the gradients were centrifuged at 100 000 RCF for 4 h at 15 °C in a Beckman Optima XPN-100 ultracentrifuge with no braking used at the end of the run. Immediately after the centrifugation, fractions of 0.5 mL were carefully taken out sequentially from top to bottom and then subjected to radioactivity assay and density measurement.

Capillary depletion was performed to quantify the BBB transport of circulating ^{125}I-ApoE3−rHDL as described previously.[39] The brain sample (100 mg) was homogenized on ice in a glass homogenizer (10 strokes) in physiologic buffer (10 mM HEPES, 141 mM NaCl, 4 mM KCl, 2.8 mM $CaCl_2$, 1 mM $MgSO_4$, 1 mM NaH_2PO_4 and 10 mM D-glucose, pH 7.4). Dextran solution was added to the homogenate to a final concentration of 13%, and the mixture was further homogenized for 3 strokes and centrifuged at 5400*g* for 15 min with the supernatant containing the brain parenchyma carefully separated from the pellet containing the brain microvasculature. Both fractions were then subjected to radioactivity assay.

Quantification of Cellular uptake of Aβ. Primary microglia, primary astrocytes and Chang liver cells were plated at a density of 5 × 10^3 cells/well, separately, in a 96-well plate in DMEM containing 10% FBS and cultured for 24 h to allow cell attachment. The cells were then incubated with FAM-Aβ (2 μg/mL) in serum-free DMEM in the absence or presence of ApoE3−rHDL (0.04, 0.2, 1, 5 μg/mL) at 37 °C for 15 min, 1 h, and 3 h, respectively. After that, the cells were washed with PBS and fixed with 3.7% formaldehyde solution for 10 min. After they were stained with Hoechst 33258 (10 μg/mL) at room temperature away from light for 10 min, the cells were finally washed three times with PBS and the cellular uptake of FAM-Aβ was quantitatively analyzed under an HCS instruments (Thermo) as described previously.[60]

Colocalization Assay. Primary microglia, primary astrocytes and Chang liver cells were plated onto 29 mm glass-bottom tissue culture dishes (MatTek, Ashland, MA) at a density of 1 × 10^5 cells/well. After overnight culture, the cells were serum-starved for 3 h and treated with 2 μg/mL FAM-Aβ in the absence or presence of ApoE3−rHDL (1 μg/mL) at 37 °C for 15 min or 3 h. Cellular distribution of FAM-Aβ was determined and analyzed under a confocal microscope (Zeiss LSM 710) with LysoTracker Red as the indicator of lysosome.

Intracellular Aβ Degradation Assay. Primary microglia, primary astrocytes and Chang liver cells were plated at a density of 2 × 10^5 cells/well in a six-well plate, separately. Twenty-four hours later, the cells were incubated with Aβ_{1-42} (2 μg/mL) in serum-free medium in the absence or presence of ApoE3−rHDL (0.2, 1, or 5 μg/mL) at 37 °C for 3 h. After washing with PBS, the cells were lysed in 1% SDS containing a protease inhibitor cocktail (Roche). The total protein content of cell lysates was analyzed *via* a Bicinchoninic acid (BCA) Protein Assay (Pierce), and the remaining intracellular Aβ_{1-42} levels were quantified with an ELISA kit and normalized to total protein in the lysates.

ApoE3−rHDL Treatment of AD Model Mice. Seven-month-old SAMP8 mice (n = 8−9 per group) were treated with ApoE3−rHDL at the DMPC dose of 5 mg/kg intravenously *via* the tail vein daily for 4 weeks with the age-matched SAMP8 and SAMR1 mice given normal saline as the negative and normal control, respectively.

Immunohistochemical Analysis. Immunohistochemical analysis was performed on formalin-fixed paraffin-embedded sections: the animals were euthanized, followed by heart perfusion with 60 mL of cold saline. The whole brains were harvested and fixed in 10% formalin, embedded in paraffin, and sectioned at 3 μm. For immunohistochemistry, the brain sections were treated with pH 6.0 citric acid for 15 min to expose the antigen, and then incubated with 0.3% peroxide in methanol for 10 min to quench the endogenous peroxidase activity. Subsequently, the sections were blocked with 5% normal goat serum in PBS containing 0.1% Triton X-100 for 1 h, and then incubated with the primary antibody in the blocking solution overnight at 4 °C. The antigens were detected by secondary antibodies using standard ABC-DAB methods. Antibody 6E10 was used to stain Aβ deposition and anti-CD45 antibody to stain activated microglia. Sections were finally counterstained with hematoxylin and images were taken and analyzed using the Leica Qwin software.

Histology. Both Nissl staining and HE staining were performed to examine the histological change in the brain. For the analysis, the brain sections were stained with cresyl violet or hematoxylin/eosin following standard protocol, and then subjected to observation and imaging under a Leica microscope. Nissl staining sections were used for quantitative analysis of neuronal injury in both the cortex and the hippocampus of the animals. And HE staining sections were applied for visualization of the robust morphological change of the cells in the brain.

Morris Water Maze (MWM) Task. The MWM setting consisted of a circular pool (diameter, 120 cm; height, 50 cm) equipped with a 9-cm platform 1 cm below the surface of water (30 cm deep) in the middle of one quadrant. For the analysis, on the first four days, the animals (n = 8−9 per group) were tested four times daily being placed into the water from the starting points which divided the pool into four quadrants with a daily different-random sequences. The cutoff time for the latency to reach the platform was 60 s. If an animal failed to reach the platform within 60 s, it was guided to the platform and stayed there for 30 s. The swimming speed, swimming path and escape latencies were recorded using a tracking system (Shanghai Jiliang Software Technology Co., Ltd.). On the fifth day, each animal was given two single probe tests with the platform removed, where the mouse was placed in water from the two starting points away from the platform by order. Spatial acuity was expressed as the percentage of time the animal spent in the quadrant where the escape platform used to be located.

Biosafety Evaluation. To evaluate the safety of ApoE3−rHDL for anti-AD therapy, following the four-week daily treatment with ApoE3−rHDL at the DMPC dose of 5 mg/kg, the animals were sacrificed and the major organs were collected, fixed, dehydrated, embedded in paraffin, serially sectioned, and stained with hematoxylin and eosin before they were subjected to optical microscopy evaluation.

Statistical Analysis. All data were expressed as mean ± SD unless otherwise indicated. For multiple-group comparison, one-way ANOVA was used followed by Bonferroni tests. Specific comparison between two groups was carried out with an unpaired Student's t-test (two tailed). Differences were considered statistically significant at $p < 0.05$.

Conflict of Interest: The authors declare no competing financial interest.

Acknowledgment. This study was supported by National Natural Science Foundation of China (No. 81373351, 81072592), National Key Basic Research Program (2010CB529800, 2013CB932500), grants from Shanghai Science and Technology

Committee (12nm0502000, 11430702200 and 12ZR1416300), Innovation Program of Shanghai Municipal Education Commission (12ZZ107), National Science and Technology Major Project 2012ZX09303001-001 and International Science & Technology Cooperation Program of China (2011DFA33180).

Supporting Information Available: Biodistribution of ^{125}I-ApoE3−rHDL and ^{125}I-ApoE3 following intravenous administration; tissue samples of SAMP8 mice treated with ApoE3−rHDL. This material is available free of charge via the Internet at http://pubs.acs.org.

REFERENCES AND NOTES

1. Serrano-Pozo, A.; Frosch, M. P.; Masliah, E.; Hyman, B. T. Neuropathological Alterations in Alzheimer Disease. *Cold Spring Harbor Perspect. Med.* **2011**, *1*, a6189.
2. Haass, C.; Kaether, C.; Thinakaran, G.; Sisodia, S. Trafficking and Proteolytic Processing of APP. *Cold Spring Harbor Perspect. Med.* **2012**, *2*, a6270.
3. Gilbert, B. J. The Role of Amyloid Beta in the Pathogenesis of Alzheimer's Disease. *J. Clin. Pathol.* **2013**, *66*, 362–366.
4. Brambilla, D.; Verpillot, R.; Le Droumaguet, B.; Nicolas, J.; Taverna, M.; Kona, J.; Lettiero, B.; Hashemi, S. H.; De Kimpe, L.; Canovi, M. PEGylated Nanoparticles Bind to and Alter Amyloid-Beta Peptide Conformation: Toward Engineering of Functional Nanomedicines for Alzheimer's Disease. *ACS Nano* **2012**, *6*, 5897–5908.
5. Liao, Y. H.; Chang, Y. J.; Yoshiike, Y.; Chang, Y. C.; Chen, Y. R. Negatively Charged Gold Nanoparticles Inhibit Alzheimer's Amyloid-Beta Fibrillization, Induce Fibril Dissociation, and Mitigate Neurotoxicity. *Small* **2012**, *8*, 3631–3639.
6. Le Droumaguet, B.; Nicolas, J.; Brambilla, D.; Mura, S.; Maksimenko, A.; De Kimpe, L.; Salvati, E.; Zona, C.; Airoldi, C.; Canovi, M. Versatile and Efficient Targeting Using a Single Nanoparticulate Platform: Application to Cancer and Alzheimer's Disease. *ACS Nano* **2012**, *6*, 5866–5879.
7. Taylor, M.; Moore, S.; Mourtas, S.; Niarakis, A.; Re, F.; Zona, C.; La Ferla, B.; Nicotra, F.; Masserini, M.; Antimisiaris, S. G. Effect of Curcumin-Associated and Lipid Ligand-Functionalized Nanoliposomes on Aggregation of the Alzheimer's Abeta Peptide. *Nanomedicine* **2011**, *7*, 541–550.
8. Mawuenyega, K. G.; Sigurdson, W.; Ovod, V.; Munsell, L.; Kasten, T.; Morris, J. C.; Yarasheski, K. E.; Bateman, R. J. Decreased Clearance of CNS Beta-Amyloid in Alzheimer's Disease. *Science* **2010**, *330*, 1774.
9. Castellano, J. M.; Kim, J.; Stewart, F. R.; Jiang, H.; DeMattos, R. B.; Patterson, B. W.; Fagan, A. M.; Morris, J. C.; Mawuenyega, K. G.; Cruchaga, C. Human apoE Isoforms Differentially Regulate Brain Amyloid-Beta Peptide Clearance. *Sci. Transl. Med.* **2011**, *3*, 57r–89r.
10. Sagare, A.; Deane, R.; Bell, R. D.; Johnson, B.; Hamm, K.; Pendu, R.; Marky, A.; Lenting, P. J.; Wu, Z.; Zarcone, T. Clearance of Amyloid-Beta by Circulating Lipoprotein Receptors. *Nat. Med.* **2007**, *13*, 1029–1031.
11. Prada, C. M.; Garcia-Alloza, M.; Betensky, R. A.; Zhang-Nunes, S. X.; Greenberg, S. M.; Bacskai, B. J.; Frosch, M. P. Antibody-Mediated Clearance of Amyloid-Beta Peptide From Cerebral Amyloid Angiopathy Revealed by Quantitative *in Vivo* Imaging. *J. Neurosci.* **2007**, *27*, 1973–1980.
12. Cramer, P. E.; Cirrito, J. R.; Wesson, D. W.; Lee, C. Y.; Karlo, J. C.; Zinn, A. E.; Casali, B. T.; Restivo, J. L.; Goebel, W. D.; James, M. J. ApoE-directed Therapeutics Rapidly Clear Beta-Amyloid and Reverse Deficits in AD Mouse Models. *Science* **2012**, *335*, 1503–1506.
13. Liu, Y. H.; Giunta, B.; Zhou, H. D.; Tan, J.; Wang, Y. J. Immunotherapy for Alzheimer Disease: The Challenge of Adverse Effects. *Nat. Rev. Neurol.* **2012**, *8*, 465–469.
14. Patil, S. P.; Ballard, R.; Sanchez, S.; Osborn, J.; Santangelo, D. J. ApoE: The Link Between Alzheimer's-related Glucose Hypometabolism and Abeta Deposition? *Med. Hypotheses* **2012**, *78*, 494–496.
15. Matsubara, E.; Sekijima, Y.; Tokuda, T.; Urakami, K.; Amari, M.; Shizuka-Ikeda, M.; Tomidokoro, Y.; Ikeda, M.; Kawarabayashi, T.; Harigaya, Y. Soluble Abeta Homeostasis in AD and DS: Impairment of Anti-Amyloidogenic Protection by Lipoproteins. *Neurobiol. Aging* **2004**, *25*, 833–841.
16. Hanson, A. J.; Bayer-Carter, J. L.; Green, P. S.; Montine, T. J.; Wilkinson, C. W.; Baker, L. D.; Watson, G. S.; Bonner, L. M.; Callaghan, M.; Leverenz, J. B. Effect of Apolipoprotein E Genotype and Diet on Apolipoprotein E Lipidation and Amyloid Peptides: Randomized Clinical Trial. *JAMA Neurol.* **2013**, *70*, 972–980.
17. Koffie, R. M.; Farrar, C. T.; Saidi, L. J.; William, C. M.; Hyman, B. T.; Spires-Jones, T. L. Nanoparticles Enhance Brain Delivery of Blood-Brain Barrier-Impermeable Probes for *in Vivo* Optical and Magnetic Resonance Imaging. *Proc. Natl. Acad. Sci. U. S. A.* **2011**, *108*, 18837–18842.
18. Zensi, A.; Begley, D.; Pontikis, C.; Legros, C.; Mihoreanu, L.; Wagner, S.; Buchel, C.; von Briesen, H.; Kreuter, J. Albumin Nanoparticles Targeted with ApoE Enter the CNS by Transcytosis and are Delivered to Neurones. *J. Controlled Release* **2009**, *137*, 78–86.
19. Zhang, Z.; Cao, W.; Jin, H.; Lovell, J. F.; Yang, M.; Ding, L.; Chen, J.; Corbin, I.; Luo, Q.; Zheng, G. Biomimetic Nanocarrier for Direct Cytosolic Drug Delivery. *Angew. Chem., Int. Ed.* **2009**, *48*, 9171–9175.
20. Sabnis, N.; Lacko, A. G. Drug Delivery *via* Lipoprotein-Based Carriers: Answering the Challenges in Systemic Therapeutics. *Ther. Delivery* **2012**, *3*, 599–608.
21. Bien-Ly, N.; Andrews-Zwilling, Y.; Xu, Q.; Bernardo, A.; Wang, C.; Huang, Y. C-Terminal-Truncated Apolipoprotein (Apo) E4 Inefficiently Clears Amyloid-Beta (Abeta) and Acts in Concert with Abeta to Elicit Neuronal and Behavioral Deficits in Mice. *Proc. Natl. Acad. Sci. U. S. A.* **2011**, *108*, 4236–4241.
22. Prevost, M.; Raussens, V. Apolipoprotein E-low Density Lipoprotein Receptor Binding: Study of Protein-Protein Interaction in Rationally Selected Docked Complexes. *Proteins* **2004**, *55*, 874–884.
23. Croy, J. E.; Brandon, T.; Komives, E. A. Two Apolipoprotein E Mimetic Peptides, ApoE(130−149) and ApoE(141−155)2, Bind to LRP1. *Biochemistry* **2004**, *43*, 7328–7335.
24. Narayanaswami, V.; Maiorano, J. N.; Dhanasekaran, P.; Ryan, R. O.; Phillips, M. C.; Lund-Katz, S.; Davidson, W. S. Helix Orientation of the Functional Domains in Apolipoprotein E in Discoidal High Density Lipoprotein Particles. *J. Biol. Chem.* **2004**, *279*, 14273–14279.
25. Khumsupan, P.; Ramirez, R.; Khumsupan, D.; Narayanaswami, V. Apolipoprotein E LDL Receptor-Binding Domain-Containing High-Density Lipoprotein: A Nanovehicle to Transport Curcumin, an Antioxidant and Anti-Amyloid Bioflavonoid. *Biochim. Biophys. Acta* **2011**, *1808*, 352–359.
26. Ng, K. K.; Lovell, J. F.; Vedadi, A.; Hajian, T.; Zheng, G. Self-Assembled Porphyrin Nanodiscs with Structure-Dependent Activation for Phototherapy and Photodiagnostic Applications. *ACS Nano* **2013**, *7*, 3484–3490.
27. Cormode, D. P.; Briley-Saebo, K. C.; Mulder, W. J.; Aguinaldo, J. G.; Barazza, A.; Ma, Y.; Fisher, E. A.; Fayad, Z. A. An ApoA-I Mimetic Peptide High-Density-Lipoprotein-Based MRI Contrast Agent for Atherosclerotic Plaque Composition Detection. *Small* **2008**, *4*, 1437–1444.
28. Tokuda, T.; Calero, M.; Matsubara, E.; Vidal, R.; Kumar, A.; Permanne, B.; Zlokovic, B.; Smith, J. D.; Ladu, M. J.; Rostagno, A. Lipidation of Apolipoprotein E Influences its Isoform-Specific Interaction with Alzheimer's Amyloid Beta Peptides. *Biochem. J.* **2000**, *348* (Pt 2), 359–365.
29. Blacklow, S. C. Versatility in Ligand Recognition by LDL Receptor Family Proteins: Advances and Frontiers. *Curr. Opin. Struct. Biol.* **2007**, *17*, 419–426.
30. Fisher, C. A.; Narayanaswami, V.; Ryan, R. O. The Lipid-Associated Conformation of the Low Density Lipoprotein Receptor Binding Domain of Human Apolipoprotein E. *J. Biol. Chem.* **2000**, *275*, 33601–33606.
31. Re, F.; Cambianica, I.; Sesana, S.; Salvati, E.; Cagnotto, A.; Salmona, M.; Couraud, P. O.; Moghimi, S. M.; Masserini, M.; Sancini, G. Functionalization with ApoE-derived Peptides Enhances the Interaction with Brain Capillary Endothelial Cells of Nanoliposomes Binding Amyloid-Beta Peptide. *J. Biotechnol.* **2010**, *156*, 341–346.

32. Bana, L.; Minniti, S.; Salvati, E.; Sesana, S.; Zambelli, V.; Cagnotto, A.; Orlando, A.; Cazzaniga, E.; Zwart, R.; Scheper, W. Liposomes Bi-Functionalized with Phosphatidic Acid and an ApoE-Derived Peptide Affect Abeta Aggregation Features and Cross the Blood-Brain-Barrier: Implications for Therapy of Alzheimer Disease. *Nanomedicine* **2013**, pii: S1549-9634(13)00684-9. DOI: 10.1016/j.nano.2013.12.001.
33. Wang, Y.; Xia, Z.; Xu, J. R.; Wang, Y. X.; Hou, L. N.; Qiu, Y.; Chen, H. Z. Alpha-Mangostin, a Polyphenolic Xanthone Derivative From Mangosteen, Attenuates Beta-Amyloid Oligomers-Induced Neurotoxicity by Inhibiting Amyloid Aggregation. *Neuropharmacology* **2012**, *62*, 871–881.
34. Innerarity, T. L.; Pitas, R. E.; Mahley, R. W. Lipoprotein-Receptor Interactions. *Methods Enzymol.* **1986**, *129*, 542–565.
35. Huwyler, J.; Wu, D.; Pardridge, W. M. Brain Drug Delivery of Small Molecules Using Immunoliposomes. *Proc. Natl. Acad. Sci. U. S. A.* **1996**, *93*, 14164–14169.
36. Huang, R.; Ke, W.; Liu, Y.; Jiang, C.; Pei, Y. The Use of Lactoferrin as a Ligand for Targeting the Polyamidoamine-Based Gene Delivery System to the Brain. *Biomaterials* **2008**, *29*, 238–246.
37. Wohlfart, S.; Khalansky, A. S.; Gelperina, S.; Begley, D.; Kreuter, J. Kinetics of Transport of Doxorubicin Bound to Nanoparticles across the Blood-Brain Barrier. *J. Controlled Release* **2011**, *154*, 103–107.
38. Deane, R.; Du Yan, S.; Submamaryan, R. K.; LaRue, B.; Jovanovic, S.; Hogg, E.; Welch, D.; Manness, L.; Lin, C.; Yu, J. RAGE Mediates Amyloid-Beta Peptide Transport Across the Blood-Brain Barrier and Accumulation in Brain. *Nat. Med.* **2003**, *9*, 907–913.
39. Triguero, D.; Buciak, J.; Pardridge, W. M. Capillary Depletion Method for Quantification of Blood-Brain Barrier Transport of Circulating Peptides and Plasma Proteins. *J. Neurochem.* **1990**, *54*, 1882–1888.
40. Pardridge, W. M. Blood-Brain Barrier Drug Targeting: The Future of Brain Drug Development *Mol. Interventions* **2003**, *3*, 90−105, 51.
41. Mehta, P. D.; Pirttila, T.; Mehta, S. P.; Sersen, E. A.; Aisen, P. S.; Wisniewski, H. M. Plasma and Cerebrospinal Fluid Levels of Amyloid Beta Proteins 1−40 and 1−42 in Alzheimer Disease. *Arch. Neurol.* **2000**, *57*, 100–105.
42. Kawarabayashi, T.; Younkin, L. H.; Saido, T. C.; Shoji, M.; Ashe, K. H.; Younkin, S. G. Age-Dependent Changes in Brain, CSF, and Plasma Amyloid (Beta) Protein in the Tg2576 Transgenic Mouse Model of Alzheimer's Disease. *J. Neurosci.* **2001**, *21*, 372–381.
43. Bricarello, D. A.; Smilowitz, J. T.; Zivkovic, A. M.; German, J. B.; Parikh, A. N. Reconstituted Lipoprotein: A Versatile Class of Biologically-Inspired Nanostructures. *ACS Nano* **2011**, *5*, 42–57.
44. Jiang, Q.; Lee, C. Y.; Mandrekar, S.; Wilkinson, B.; Cramer, P.; Zelcer, N.; Mann, K.; Lamb, B.; Willson, T. M.; Collins, J. L. ApoE Promotes the Proteolytic Degradation of Abeta. *Neuron* **2008**, *58*, 681–693.
45. Koistinaho, M.; Lin, S.; Wu, X.; Esterman, M.; Koger, D.; Hanson, J.; Higgs, R.; Liu, F.; Malkani, S.; Bales, K. R. Apolipoprotein E Promotes Astrocyte Colocalization and Degradation of Deposited Amyloid-Beta Peptides. *Nat. Med.* **2004**, *10*, 719–726.
46. Lee, C. Y.; Tse, W.; Smith, J. D.; Landreth, G. E. Apolipoprotein E Promotes Beta-Amyloid Trafficking and Degradation by Modulating Microglial Cholesterol Levels. *J. Biol. Chem.* **2012**, *287*, 2032–2044.
47. Ghosh, R. N.; Grove, L.; Lapets, O. A Quantitative Cell-Based High-Content Screening Assay for the Epidermal Growth Factor Receptor-Specific Activation of Mitogen-Activated Protein Kinase. *Assay Drug Dev. Technol.* **2004**, *2*, 473–481.
48. Hone, E.; Martins, I. J.; Fonte, J.; Martins, R. N. Apolipoprotein E Influences Amyloid-Beta Clearance from the Murine Periphery. *J. Alzheimer's Dis.* **2003**, *5*, 1–8.
49. Butterfield, D. A.; Poon, H. F. The Senescence-Accelerated Prone Mouse (SAMP8): A Model of Age-Related Cognitive Decline with Relevance to Alterations of the Gene Expression and Protein Abnormalities in Alzheimer's Disease. *Exp. Gerontol.* **2005**, *40*, 774–783.
50. Wyss-Coray, T. Inflammation in Alzheimer Disease: Driving Force, Bystander or Beneficial Response? *Nat. Med.* **2006**, *12*, 1005–1015.
51. Sondag, C. M.; Dhawan, G.; Combs, C. K. Beta Amyloid Oligomers and Fibrils Stimulate Differential Activation of Primary Microglia. *J. Neuroinflammation* **2009**, *6*, 1.
52. West, M. J.; Coleman, P. D.; Flood, D. G.; Troncoso, J. C. Differences in the Pattern of Hippocampal Neuronal Loss in Normal Ageing and Alzheimer's Disease. *Lancet* **1994**, *344*, 769–772.
53. Takeda, T.; Matsushita, T.; Kurozumi, M.; Takemura, K.; Higuchi, K.; Hosokawa, M. Pathobiology of the Senescence-Accelerated Mouse (SAM). *Exp. Gerontol.* **1997**, *32*, 117–127.
54. Floden, A. M.; Li, S.; Combs, C. K. Beta-Amyloid-Stimulated Microglia Induce Neuron Death *via* Synergistic Stimulation of Tumor Necrosis Factor Alpha and NMDA Receptors. *J. Neurosci.* **2005**, *25*, 2566–2575.
55. Saura, J.; Tusell, J. M.; Serratosa, J. High-Yield Isolation of Murine Microglia by Mild Trypsinization. *Glia* **2003**, *44*, 183–189.
56. Kayed, R.; Head, E.; Thompson, J. L.; McIntire, T. M.; Milton, S. C.; Cotman, C. W.; Glabe, C. G. Common Structure of Soluble Amyloid Oligomers Implies Common Mechanism of Pathogenesis. *Science* **2003**, *300*, 486–489.
57. Lambert, M. P.; Barlow, A. K.; Chromy, B. A.; Edwards, C.; Freed, R.; Liosatos, M.; Morgan, T. E.; Rozovsky, I.; Trommer, B.; Viola, K. L. Diffusible, Nonfibrillar Ligands Derived From Abeta1−42 are Potent Central Nervous System Neurotoxins. *Proc. Natl. Acad. Sci. U. S. A.* **1998**, *95*, 6448–6453.
58. Stine, W. J.; Dahlgren, K. N.; Krafft, G. A.; LaDu, M. J. *In Vitro* Characterization of Conditions for Amyloid-Beta Peptide Oligomerization and Fibrillogenesis. *J. Biol. Chem.* **2003**, *278*, 11612–11622.
59. Chapman, M. J.; Goldstein, S.; Lagrange, D.; Laplaud, P. M. A Density Gradient Ultracentrifugal Procedure for the Isolation of the Major Lipoprotein Classes From Human Serum. *J. Lipid Res.* **1981**, *22*, 339–358.
60. Song, Q.; Yao, L.; Huang, M.; Hu, Q.; Lu, Q.; Wu, B.; Qi, H.; Rong, Z.; Jiang, X.; Gao, X. Mechanisms of Transcellular Transport of Wheat Germ Agglutinin-Functionalized Polymeric Nanoparticles in Caco-2 Cells. *Biomaterials* **2012**, *33*, 6769–6782.